MEASUREMENT AND SIMULATION ANALYSIS OF CO_2 LEAKAGE AT THE CRYSTAL GEYSER SITE AND RECONCILIATION OF THE MECHANISMS FOR THE AMOUNT OF FLUX FROM THE GEYSER AND ADJACENT FAULTS

by

Richard T. Lyons

A thesis submitted to the faculty of
The University of Utah
in partial fulfillment of the requirements for the degree of

Master of Science

Department of Civil and Environmental Engineering

The University of Utah

May 2015

The University of Utah Graduate School

STATEMENT OF THESIS APPROVAL

The thesis of **Richard T. Lyons**

has been approved by the following supervisory committee members:

Brian McPherson	, Chair	**30 June 2014** Date Approved
Weon Shik Han	, Member	**24 June 2014** Date Approved
Steven Bartlett	, Member	Date Approved

and by **Michael Barber**, Chair/Dean of

the Department/College/School of **Civil and Environmental Engineering**

and by David B. Kieda, Dean of The Graduate School.

ABSTRACT

Global warming enhanced by anthropogenic CO_2 is an ever-increasing concern to scientists, policy makers, and the public at large. One plausible method of mitigating growing emissions is to inject CO_2 into subsurface aquifers, which have large storage potential, thus helping diminish the accumulation of CO_2 in the atmosphere. The earth stores and releases large amounts of CO_2 naturally. Studying known natural sources and leaks of CO_2 can help to better understand deep-saline CO_2 storage. This study focuses on the effects of barometric pressure on surface CO_2 leakage through a fault from subsurface CO_2 storage. We measured the natural release of CO_2 at the Little Grand Wash Fault near the Crystal Geyser, a cold-water geyser located near Green River, Utah. We observed that barometric pressure affects CO_2 flux in two different manners, an immediate direct and inverse effect and a longer, 21.5-hour delayed indirect relationship.

Two one-dimensional simulation models were developed using the fluid flow equation for vertical flow. Both models simulated gaseous phase CO_2 flow from a fully saturated reservoir to the surface. The first model was run to identify a range of permeabilities that resulted in the mean observed surface flux. The second model was run to understand the indirect and time-lagged influence of barometric pressure on the CO_2 fault.

The observed barometric pressure was propagated through the subsurface and

directly added to or subtracted from the reservoir pressure and was able to mimic the resulting change in observed CO_2 flux. Reservoir pressures included a range from minimum pressure necessary to induce flow to the surface, through hydrostatic pressure to artesian conditions established by water infiltration that recharges the CO_2 reservoir from two elevations much higher than the seepage site.

Even though barometric pressure flux ranges can be accounted for in the near subsurface, the simulation results from both models imply that daily barometric pressure fluctuations do not greatly affect the leakage rates of deeply-stored CO_2. Conversely, the 21.5-hour trend can be shown to directly affect the surface seepage of CO_2 in a partially confined reservoir.

TABLE OF CONTENTS

LIST OF FIGURES

ACKNOWLEDGEMENTS

I would like to thank my advisor, Dr. Brian McPherson for his unending and contagious enthusiasm and for his great knowledge, which has been helpful and inspiring during my studies and research. I would not have been directed toward the study of subsurface fluid flow without his mentoring and friendship.

I would also like to thank my wife for her continued support throughout the long hours, the late nights, and the rewrites that have led to completing this work.

CHAPTER 1

INTRODUCTION

1.1 Background

With continued realization that anthropogenic CO_2 is polluting the atmosphere and potentially causing climatic shifts around the world (IPCC, 2007), there has been renewed interest in ways to counteract the increasing emissions, short of completely shifting energy production away from hydrocarbon usage, which, in 2012, made up 85% of worldwide electricity sources (Mills, 2012). In order to stem this accelerated accumulation of anthropogenic CO_2, one approach is to capture CO_2 at its source and dispose of it into deep saline aquifers, mature hydrocarbon reservoirs, or the ocean (Gunter et al., 1998; Gupta et al., 1999; Weir et al., 1995; White et al., 2001). However, for CO_2 sequestration to be used as an effective means of long-term storage, it must also be shown to be reasonably safe, i.e., the CO_2 should remain in its storage, at depth, from hundreds to thousands to millions of years (IPCC, 2005).

A few safety concerns of CO_2 sequestration include seismicity, integrity of underground sources of drinking water, and seepage of CO_2 from the surface of the earth through man-made wells, as well as natural faults and fissures (DOE, 2010; Gale, 2004; Nicol et al., 2011; Oldenberg and Unger, 2003).

Options are limited for studying known leakage from existing engineered, CO_2-

storage sites. Therefore, a currently used method to assess the viability of long-term sequestration is to study the CO_2 emitted from a natural CO_2 reservoir as an analog to an engineered system (Evans et al., 2004; Gouveia and Friedmann, 2006; Pearce et al., 1996). The Colorado Plateau, which covers sections of the states of Utah, Colorado, New Mexico, and Arizona, has natural CO_2 storage as well as CO_2-seepage sites that have been studied for various reasons and may give a better understanding of how CO_2 injected into deep-saline aquifers might behave (Campbell, 1978; Evans et al., 2004; Gouveia and Friedmann, 2006; Jeandel et al., 2010).

Among the sites of interest in the Colorado Plateau is the Little Grand Wash fault (LGW) and the associated Crystal Geyser, a particularly interesting artesian fed cold-water geyser; the driving mechanism of the geyser is thought to be associated with leakage from a deep CO_2 reservoir (Glennon and Pfaff, 2005; Waltham, 2001) (Figure 1.1). Within the Colorado Plateau lies the sedimentary Paradox Basin distinguished by

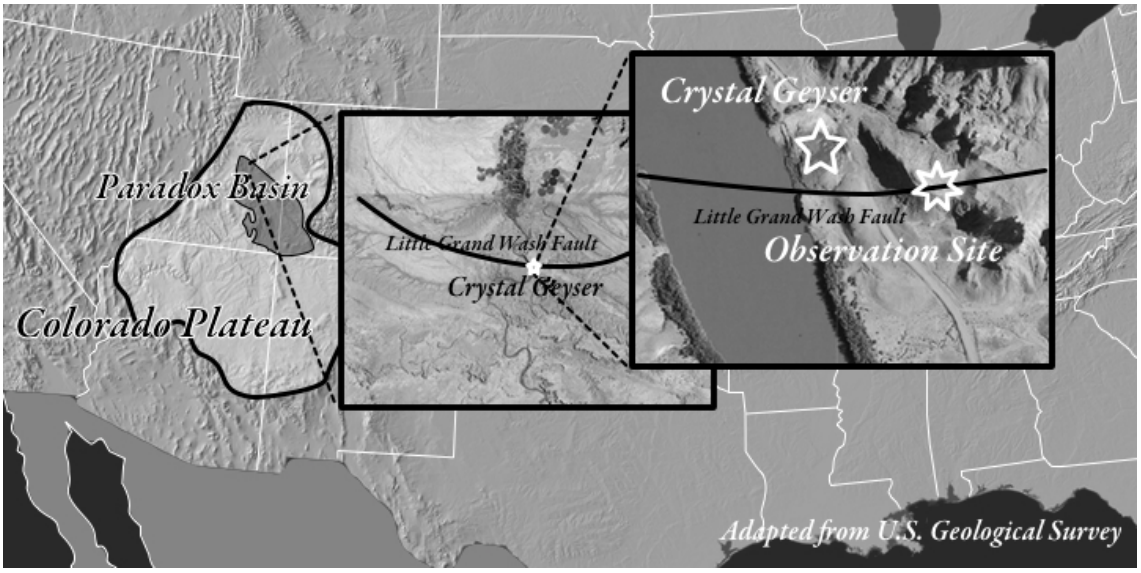

Figure 1.1 Map of observation site with Crystal Geyser

thick sequences of evaporate, carbonate, and clastic sediments (Hintze, 1993). At the north end of the Paradox Basin the LGW cuts the salt-uplifed Green River anticline and creates a lateral barrier to groundwater flow. Gaseous CO_2 and CO_2-saturated groundwater collect at the crest of the Green River anticline and migrate to the surface through fractures and fissures of the LGW damage zone (Burnside et al., 2013; Campbell and Baer, 1978; Dockrill and Shipton, 2010; Kampman et al., 2014). Crystal Geyser lies in the damage zone of the LGW (Baer and Rigby, 1978).

1.2 Goals

The primary goal of this study was to measure and analyze CO_2 leakage, observed as flux, from the Little Grand Wash Fault (LGWF) at the Crystal Geyser site and to reconcile the mechanisms for the corresponding observed surface CO_2 flux. Studying known natural sources and leaks of CO_2 can help to better understand this phenomenon that may affect the safety of deep-saline CO_2 storage. This was achieved through the following steps:

a. Measured the CO_2 surface flux emitted from the LGWF at a predetermined location near the Crystal Geyser.
b. Analyzed the data and assessed correlations between barometric pressure and surface flux.
c. Developed simulation models to analyze flow from the base of the CO_2 reservoir through a rock fracture to the earth's surface to interpret conditions and physical properties necessary to induce the observed fluxes. Specifically, determined what combination of conditions, both at

depth and at the surface, that will induce the magnitude and variation of CO_2 flux emissions measured at the LGWF site.

CHAPTER 2

NATURAL ANALOG

2.1 Atmospheric Effects on Groundwater

Body forces, such as barometric pressure, have been shown to affect water table levels in various systems, and the effect is especially strong in confined aquifers (Hare and Morse, 1997; Spane, 1999). Furthermore, failure to account for barometric pressure can introduce errors and noise in water table measurements (Rasmussen and Crawford, 1997). In a confined aquifer, fluctuations in water level, pressure head, or fluid flux can be observed as a direct result of barometric pressure fluctuations (Batu, 1998; Spane, 1999). Barometric pressure acts on the entire aquifer and not just the water surface within a well. The same relationship should exist for all fluids in the aquifer. The transmittal of atmospheric pressure from the surface to the confining interface is nearly instantaneous (Batu, 1998). Barometric pressure exerts pressure on the earth, and this force causes a response, often time delayed, on the fluid, whether it be exhibited in the water surface elevation in a well or in the surface fluid flux. As air pressure increases, it effectively compacts the surface layers, thus forcing fluid in a well to rise and associated fluid flux to increase, but the atmospheric pressure also acts directly on the fluids involved, causing water in a well to lower and flux levels to decrease. Conversely, as air pressure decreases, the surface layers rebound (swell, in effect),

therefore decreasing the level of the water in relation to the earth's surface and simultaneously causing the water level in the well to rise.

2.2 Methodology

Several trips to and around the Little Grand Wash fault were conducted to measure CO_2 outgassing from the fault damage zone, but the collected data covered too short of a time span to analyze easily. Thus a longer field campaign, from July 7, 2011 through July 20, 2011, was completed. Previous surveys had mapped out spots of high flux readings. An infrared CO_2/H_2O domed-chamber gas analyzer (LI-COR, Inc. Model LI-8100) was installed near the previously-identified spots of high CO_2 flux, and it collected continuous data throughout the duration of the field campaign. The CO_2/H_2O gas analyzer recorded CO_2 flux in micromole per square meter per second ($\mu mol/m^2 \bullet s$), mean pressure in Pascals (Pa), and temperature in degrees Celsius (°C). For purposes of this study, flux was reported in $g/m^2 \bullet day$ and surface pressure was adjusted to a sea-level equivalent. The effects of temperature on flux were not evaluated for this study.

2.3 Data Analysis

Brief analysis of data from the first few days of observations showed a seemingly diurnal trend to pressure data, which was expected, so a simple graph of barometric pressure and CO_2 flux versus time was plotted (Figure 2.1). Regression analysis between pressure and flux revealed that a fourth order polynomial had the best fit with R^2 of only 0.19793, indicating no apparent correlation (Figure 2.2), so further analyses were undertaken to explore various possibilities.

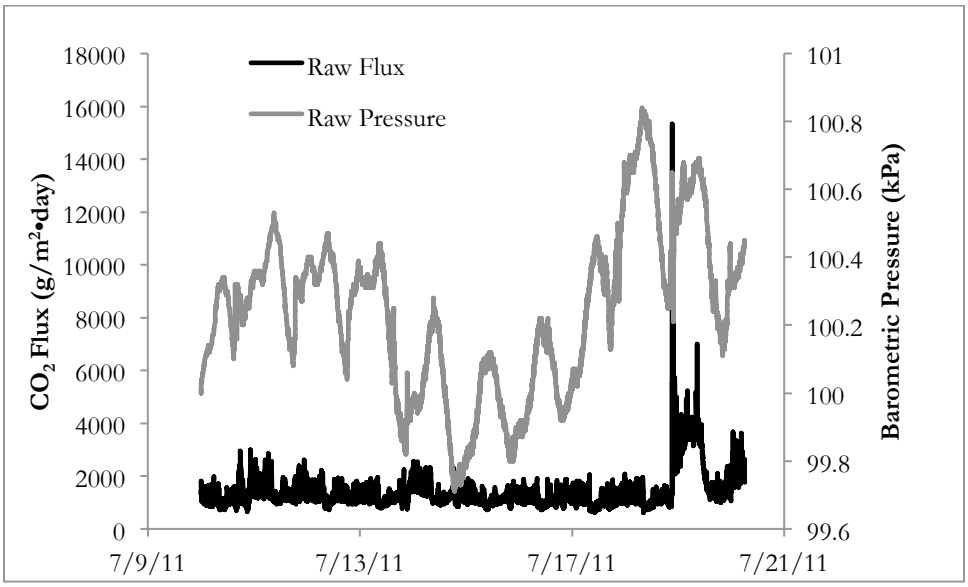

Figure 2.1 CO_2 flux and barometric pressure versus time

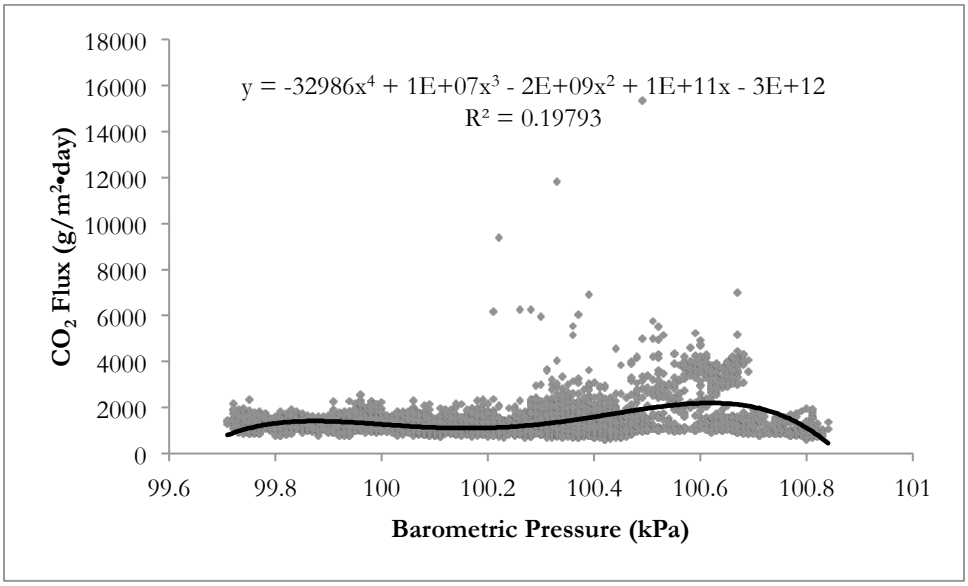

Figure 2.2 CO_2 flux versus barometric pressure

Variability in the data can make finding trends and relationships difficult. So, to help correlate flux and pressure, a symmetric moving average with 101 points, 50 points on either side of each given value, was run to smooth the data (Figure 2.3). A symmetric moving average uses an equal number of data on either side of a given point and then computes an average of those points, in this case 101 points. A new averaged value is computed for every point in the data and replaces the original value. The result was corroborated by the Central Limit Theorem by assuring that the newly calculated means of smoothed flux at 1401 g/m^2•day and smoothed pressure at 100.24 kPa approximated the means of raw flux at 1407 g/m^2•day and raw pressure at 100.24 kPa. Again, no visible correlation was confirmed (Figure 2.4).

Abnormally high readings of both CO_2 flux and barometric pressure were observed in their respective data sets, but at different times. The barometric pressure anomaly occurred at the same time that a microburst storm passed over the site on 7/18/2011 at

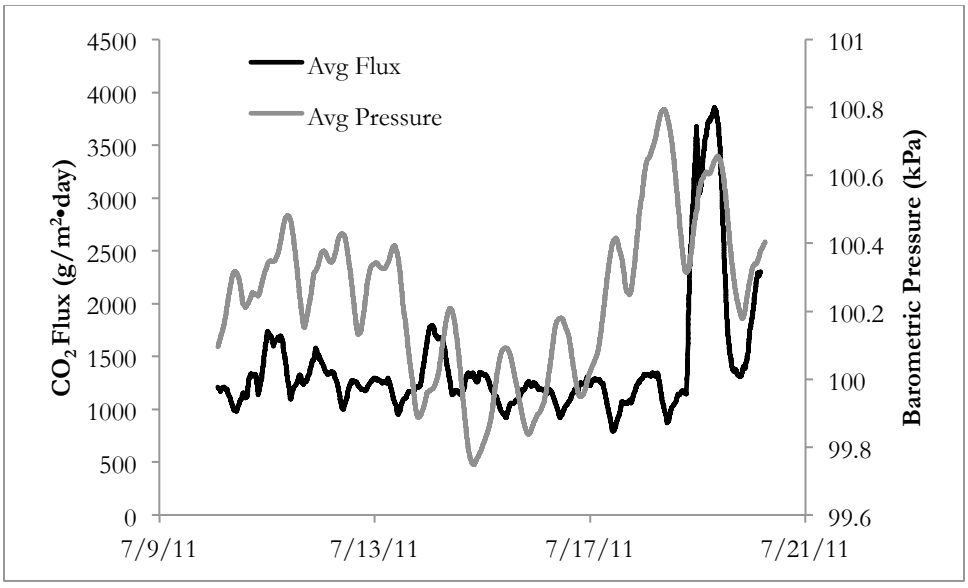

Figure 2.3 Flux and pressure, both smoothed, versus time

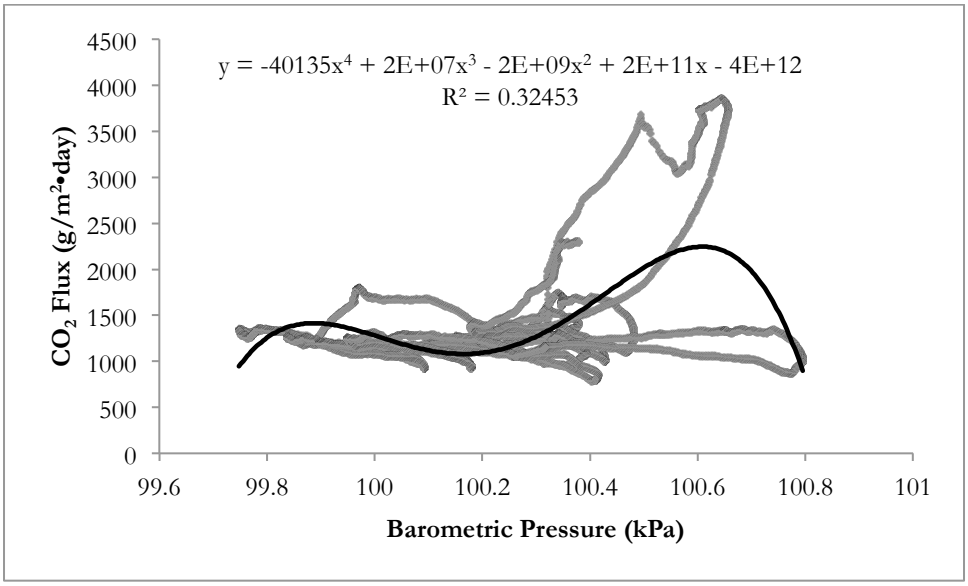

Figure 2.4 CO_2 flux versus barometric pressure after smoothing of data

7:40 am. The flux anomaly occurred at 10:20 pm, or 14:40 after the storm passed. In an attempt to relate the pressure data and the storm event, the pressure data were lagged 14:40 (Figure 2.5). The statistical correlation, or R-squared value, increased to 0.43145, but was still too low to indicate a definite relationship (Figure 2.6).

Even though lag was initially based only on the raw data, it became apparent that noise in the raw data set might be obfuscating the broader general trend in the data and that a better fit might result by lagging pressure to match the highest peaks of the smoothed data (Figure 2.7). The lagged pressure data were then graphed against CO_2 flux, which increased R^2 to 0.83194, indicating a highly probable correlation (Figure 2.8).

Around Crystal Geyser, the barometric pressure data exhibited a diurnal cycle of roughly 24 hours. A similar trend was noted regarding the CO_2 flux data. The daily cyclic nature of both sets of data indicated a possible correlation. A "zoomed in" view

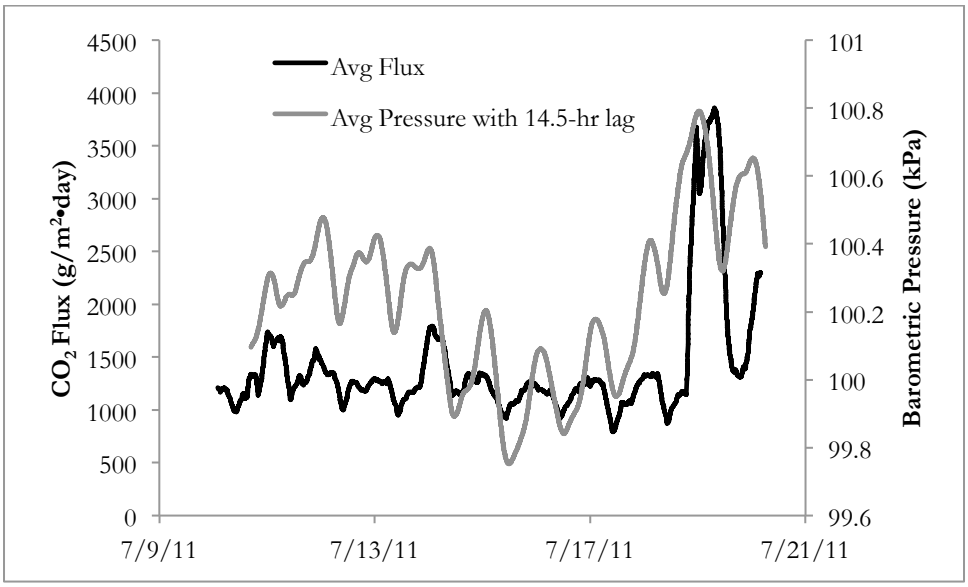

Figure 2.5 Flux and 14.5-hour lagged pressure, both smoothed, versus time

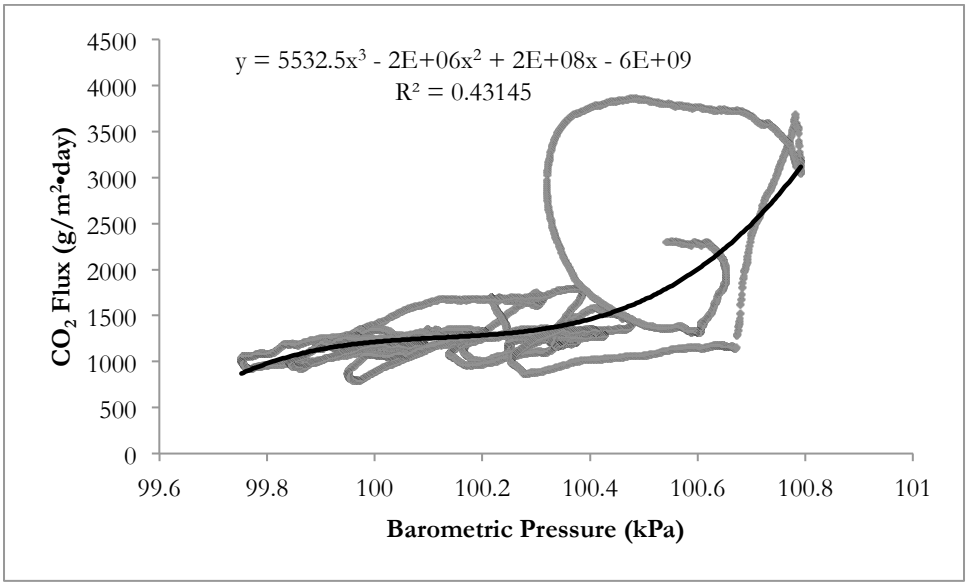

Figure 2.6 Flux versus 14.5-hour lagged pressure, both smoothed

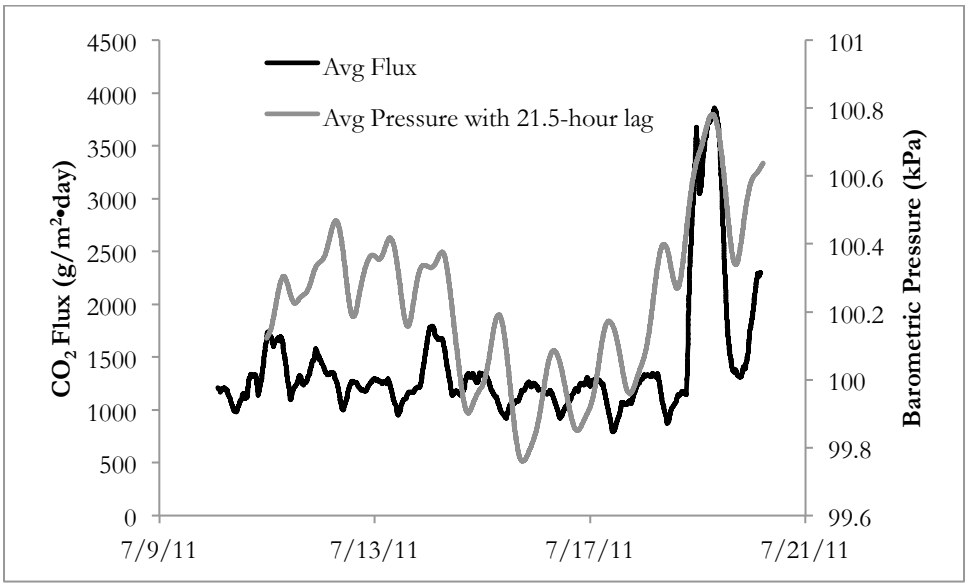

Figure 2.7 Flux and 21.5-hour lagged pressure, both smoothed, versus time

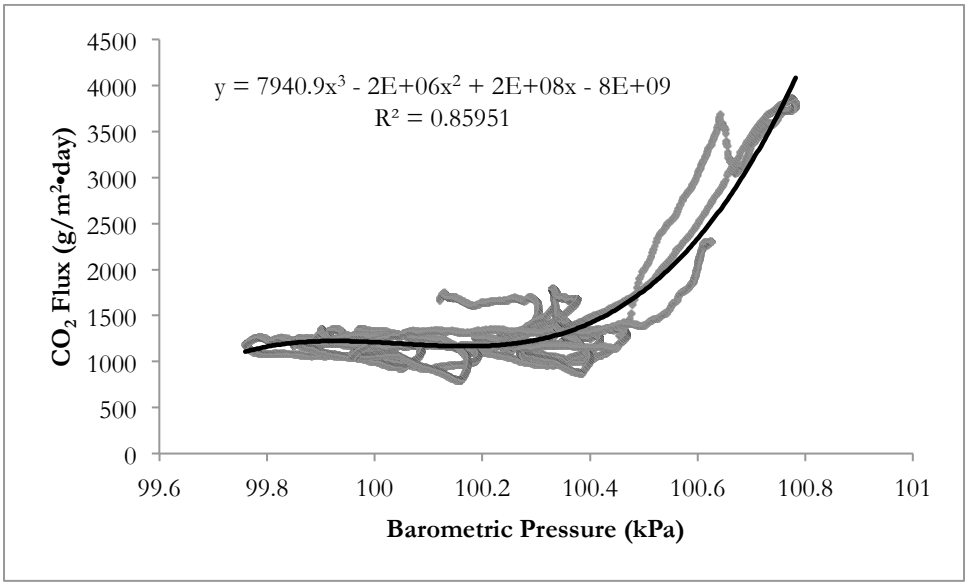

Figure 2.8 Flux versus 21.5-hour lagged pressure, both smoothed

of the graph of flux and pressure versus time seemed to also suggest a definitive relationship (Figure 2.9). The axis of the flux readings was inverted to highlight the corresponding peaks and valleys.

The data were then divided into segments of various lengths, and each segment was analyzed for trends. In nearly every case, the daily data for 6-hour long segments intimated a similar yet inverse relationship between CO_2 flux and barometric pressure and exhibited a seemingly high correlation using the smoothed data. In several instances, successive 6-hour long segments showed significant correlation (Figure 2.10 and Figure 2.11).

2.4 Data Interpretation

The results of this basic data analysis suggest that two separate mechanisms are at play, and both are driven by barometric pressure. One mechanism of pressure

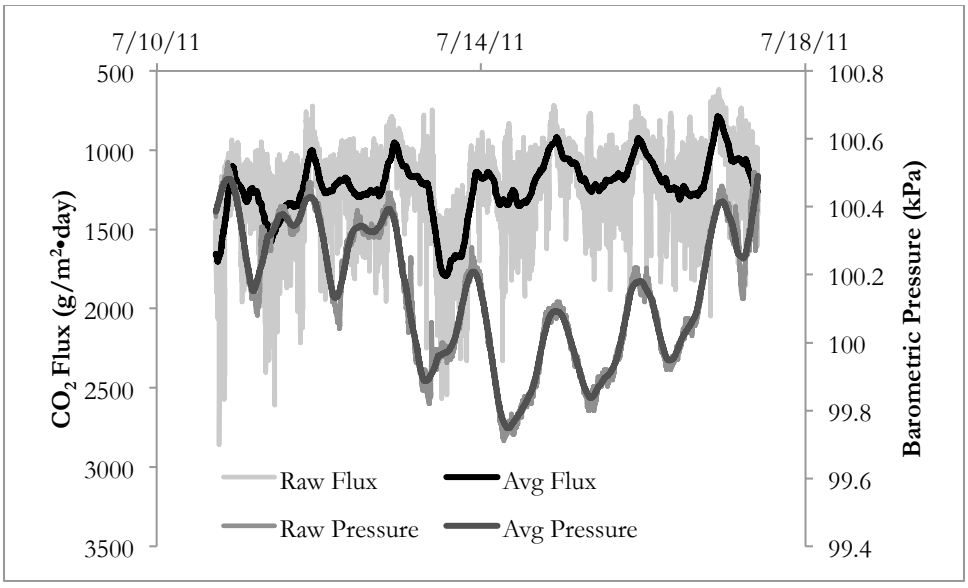

Figure 2.9 Flux and pressure versus time for 6 days

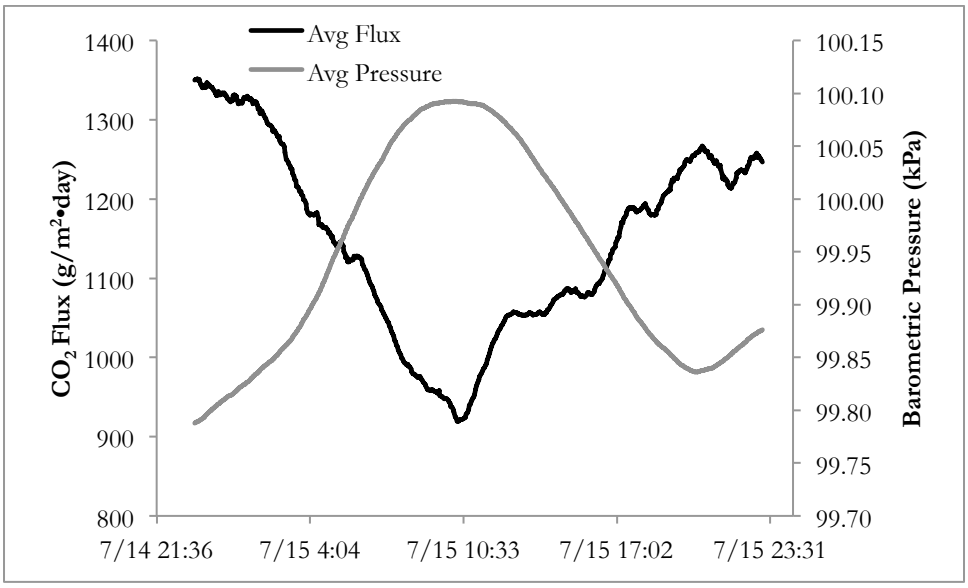

Figure 2.10 Pressure and flux versus time for four consecutive 6-hour segments

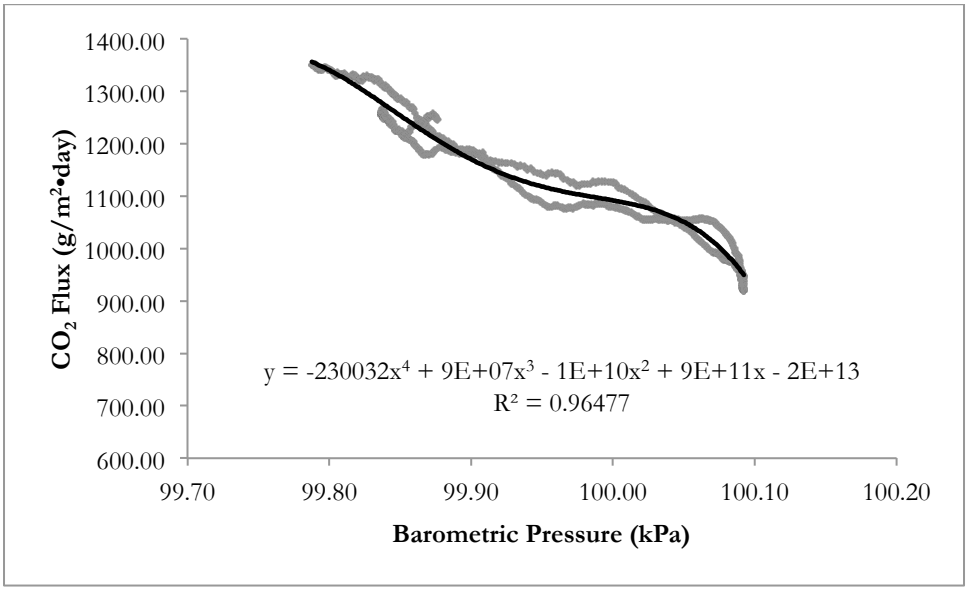

Figure 2.11 Pressure versus flux for four consecutive 6-hour segments

variability takes roughly 21.5 hours to act on the CO_2 flux response and has a direct correlation—as pressure increases flux increases. The other mechanism is immediate and has an inverse correlation—as pressure increases, flux decreases, but this correlation is only consistently valid for short time frames, around 6 hours. This can be interpreted that barometric pressure acts on at least two different materials.

Barometric pressure directly and immediately impacts CO_2 flux as it escapes from the ground. Therefore, as the air pressure increases, it impedes the escape of gas from the subsurface, and as air pressure decreases, there is less force to hinder the escape of CO_2 and more gas is released in the same period of time (Figure 2.12).

In contrast, the 21.5-hour lagged response suggests that high barometric pressure forces the surface of the earth to compress, increasing pressure in the pore space. This increase drives the CO_2 toward the more permeable fault, which offers a pathway for the CO_2 to escape. When the pressure is diminished, the earth decompresses, increasing pore space and thus releasing less gas (Figure 2.13).

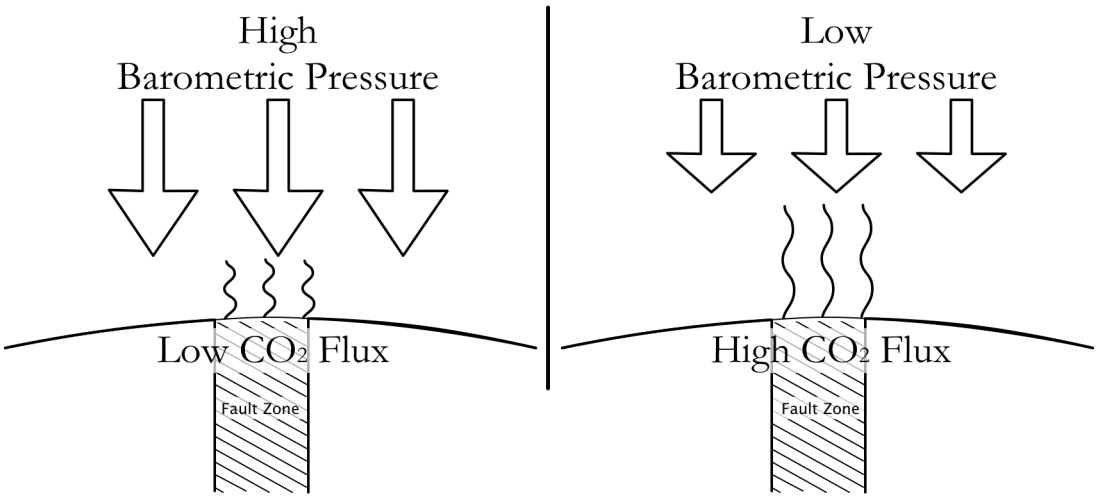

Figure 2.12 Immediate and inverse correlation between pressure and flux

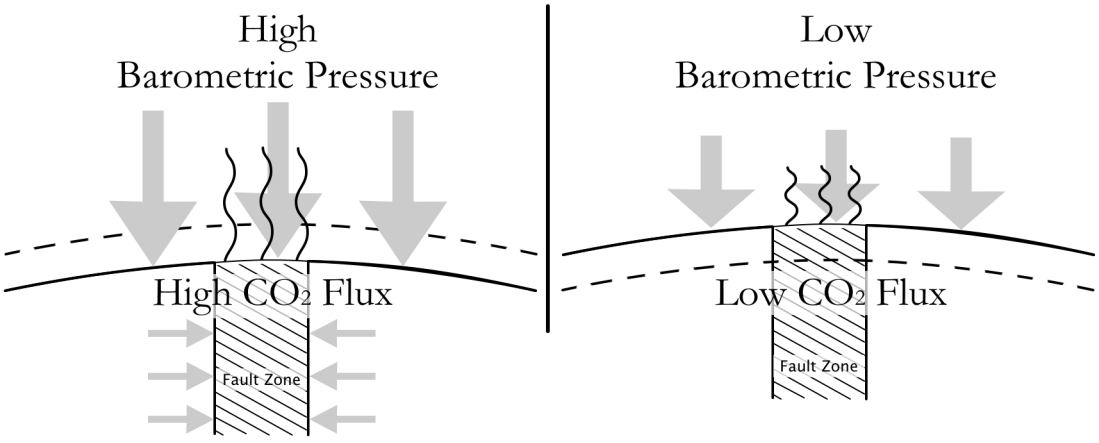

Figure 2.13 21.5-hour lag and direct correlation between pressure and flux

CHAPTER 3

COMPUTER MODEL AND SIMULATIONS

3.1 Fundamental Fluid Flow

In 1856, in Dijon, France, Henry Darcy wrote about laboratory experiments that he performed in the hopes of describing the flow of water through a sand column (Freeze, 1994). These simple experiments led directly to the formulation of the simple yet fundamental theory that describes fluid flow through a saturated medium, or Darcy's Law. The empirically derived equation has the form

$$Q = -KA\frac{dh}{dl} \tag{3.1}$$

This formula states that the volumetric flow of water (Q) is equal to a hydraulic constant (K) multiplied by the cross-sectional area of the medium (A) multiplied by the hydraulic gradient (dh/dl). The hydraulic constant is specific to a given porous medium and is also referred to as hydraulic conductivity because it expresses the ability of a medium to allow the flow-through transmission of fluid. The hydraulic gradient describes the change in pressure head over the change in length of the column of the porous medium. Pressure head (H) is calculated by the equation

$$H = \frac{p}{\rho g} + z \tag{3.2}$$

where p is pressure, ρ is the density of the flowing fluid, g is the acceleration due to gravity, and z is the height above a given point, or datum.

The movement of fluid through the subsurface is described by the general one-dimensional fluid flow equation

$$\frac{\partial}{\partial z}\left(\frac{\rho_c k_{rc} k}{\mu_c}\frac{\partial}{\partial z}(p + \rho_c g z)\right) + \frac{\partial}{\partial z}\left(\frac{\rho_w k_{rw} k}{\mu_w}\frac{\partial}{\partial z}(p + \rho_w g z)\right) = \frac{\partial(n\rho_f)}{\partial t} \tag{3.3}$$

In a simple vertical column model, the x and y direction are neglected and the vertical movement is governed by density (ρ), pressure (p), permeability (k), relative permeability (k_r), and porosity (n). The right hand side fluid density is defined as $\rho_f = S_c\rho_c + S_w\rho_w$, where S stands for saturation. The subscript c stands for carbon, w for water, and f for combined fluids. The fluid flow equation is derived using the conservation of mass equation $M_{in} - M_{out} = \Delta M/\Delta t$, where M is mass and t is time, along with continuity equation for vertical flow: $(\partial v_z)/\partial z = 0$, where v_z is fluid velocity, and then substituting out v_z for q in the pressure form of the darcy velocity in the vertical direction

$$q = \frac{Q}{A} = -K\frac{dh}{dl} = -\frac{k}{\mu}\left(\frac{\partial p}{\partial z} + \rho g\right) \tag{3.4}$$

The simulations propagated the atmospheric pressure from the surface through the

subsurface over time. One simulation was run for each of several barometric pressures, determined by the barometric pressure at the Crystal Geyser site during the data-collection time. Pressure in the reservoir was varied according to hydrostatic pressure ($P = \rho g h$), generated due to the elevation difference between the aquifer and the water recharge area in the San Rafael Swell. The propagated pressure head generated due to the elevation of the water infiltrated at the recharge site is exhibited as artesian conditions in the reservoir at the observation site. The pressure within each cell was calculated as the gradient between the surface and the reservoir pressure.

3.2 Numerical Models

In order to interpret and quantify both the direct and indirect effects of barometric pressure on CO_2 leakage, a numerical simulation approach was undertaken. Simulations were executed using the TOUGH2 code (Pruess et al., 1999) with the ECO2N fluid property module (Pruess, 2005), which accounts for CO_2 in two fluid phases—an aqueous phase and a gaseous phase, but which cannot represent transitions between super and subcritical conditions. In the deep-saline aquifers considered for long-term storage, high pressures and temperatures necessitate that CO_2 be injected in its supercritical phase to match natural conditions in the subsurface. As a supercritical fluid, CO_2 exhibits a density similar to the liquid phase and a low viscosity similar to the gas phase. After injection, as the fluid plume migrates up along faults and fissures, both the pressure and temperature decrease. These reductions cause the CO_2 to change phase from supercritical to subcritical (below the critical point of 31.04 °C and 7.382 MPa). At this point, as well as when CO_2 reaches the earth's surface, it is, under normal

conditions, a gas (Figure 3.1).

Therefore, in these simulations, since the majority of the CO_2-charged groundwater originates in the Navajo sandstone and to stay within the parameters of the ECO2N simulator fluid module, the pressure and temperature have been limited to fall within the subcritical range where CO_2 was treated solely in the gaseous phase, with some CO_2 dissolved in water (Dockrill and Shipton, 2010; Kampman et al., 2014).

3.3 Conceptual Model

The CO_2 leakage that feeds the Crystal Geyser has been speculated to originate from the Navajo Sandstone at a depth of around 215 meters (Bear and Rigby, 1978; Campbell, 1978; Waltham, 2001). More recent chemical analysis, however, suggests that a deeper reservoir of stored CO_2, located in the Wingate formation at a depth of around 480 meters, is also feeding the site although in lesser quantities (Heath, 2004; Kampman et al., 2014; Wilkinson et al., 2009) (Figure 3.2).

Due to the proximity of Crystal Geyser and the observation site on LGW and due to

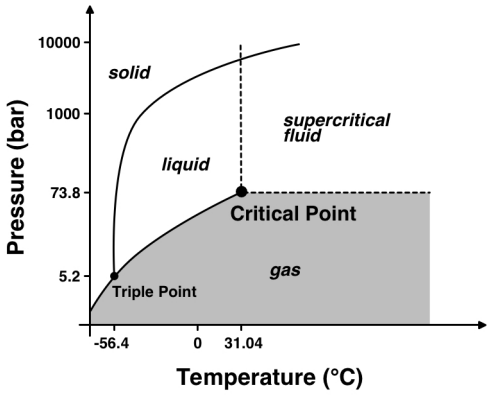

Figure 3.1 CO_2 phase diagram. Shaded area indicates gas range

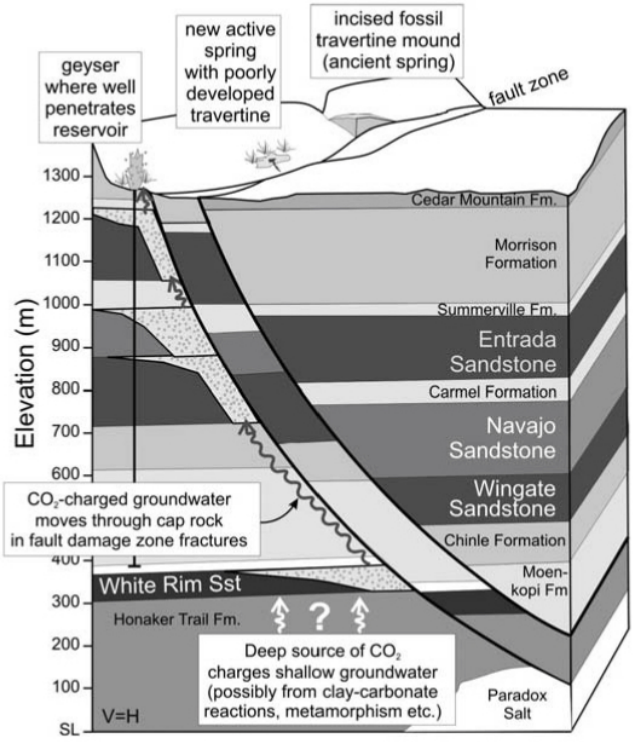

Figure 3.2 Cross section of the Little Grand Wash fault zone (Vrolijk et al., 2005)

the sheer size of the Navajo and Wingate formations, CO_2 at both locations have a similar source (Kampman et al., 2014; Wilkinson et al., 2009).

It has also been postulated and corroborated that the Navajo and Wingate formations around the Crystal Geyser have been recharged by rainwater from the San Rafael Swell (Campbell, 1978; Waltham, 2001; Wilkinson et al., 2009) (Figure 3.3).

A potentiometric map of the region between Crystal Geyser and the San Rafael Swell indicates the general area of surface recharge (Figure 3.4). From this map, surface elevations of possible water infiltration locations were determined, and hydrostatic conditions were then calculated for the Wingate and Navajo reservoirs. Hydrostatic pressure calculated from the two elevations obtained from the San Rafael Swell recharge area, 1525 meters and 1650 meters, were exhibited as artesian conditions at the

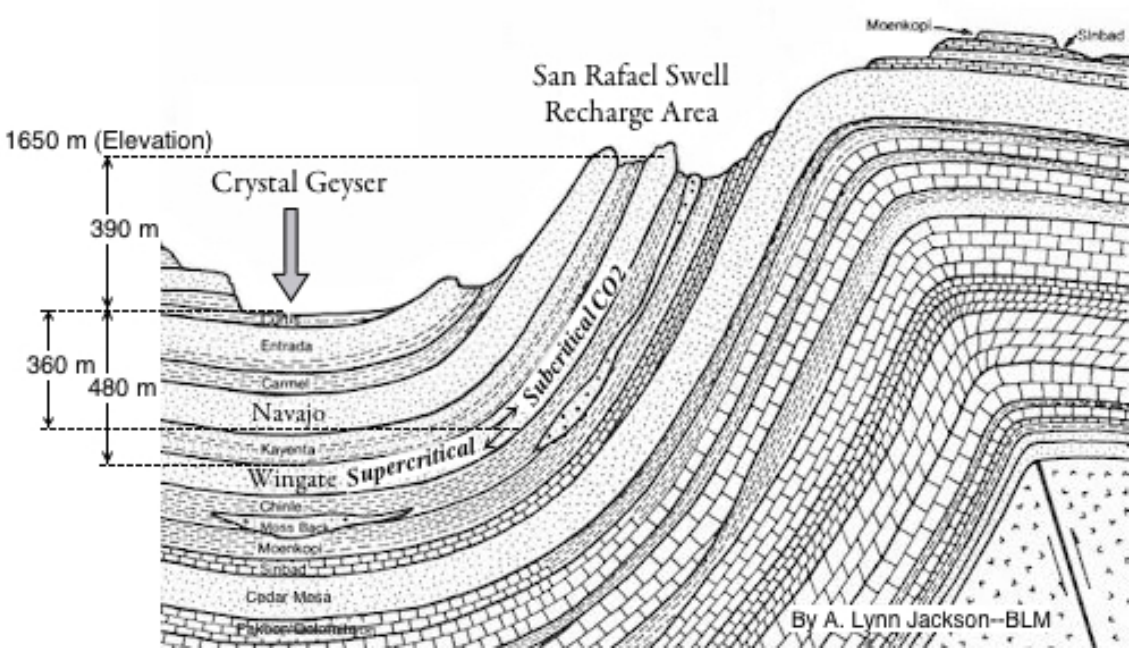

Figure 3.3 Cross section of recharge area for CO_2 reservoir (adapted from Kelsey, 2014)

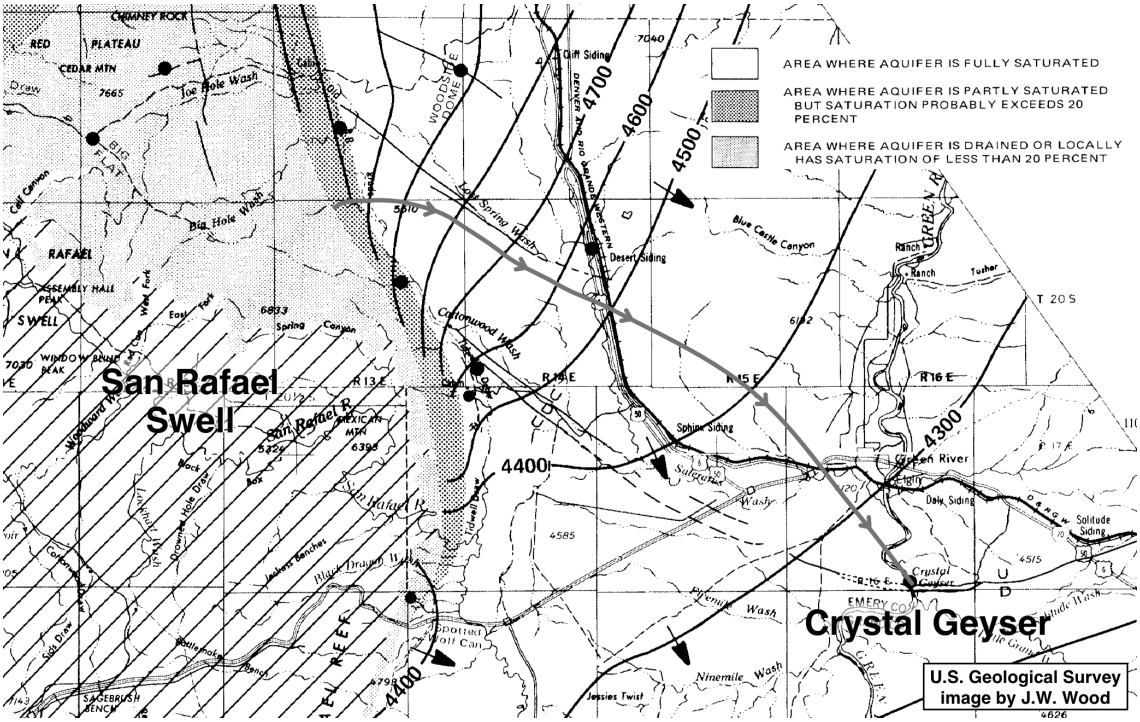

Figure 3.4 Groundwater potentiometric map (adapted from Hood and Patterson, 1984)

fault site. Reservoir pressures were calculated solely based on elevation differences. Due to the simplicity of this study and to the impracticality of gathering accurate pressure data from within the reservoir, any localized reservoir pressure build up due to CO_2 exsolution was neglected for this study.

To simulate the effects of varying barometric pressure on a fault system leaking CO_2, two simple one-dimensional vertical models were created—a permeability model and a pressure model (Figure 3.5). P_S signifies barometric pressure at the surface, P_R signifies reservoir pressure at depth, T is temperature, ρ is fluid density, Φ is porosity, k is permeability, λ represents heat conductivity, C denotes specific heat, and XCO2 is the mass fraction of CO_2 in each cell.

In all model simulations, variations in cell width and length created no measurable difference in results, so a size of 1 meter was used for convenience in calculations. In the permeability model, cell depths of 10 meters or less had results that varied insignificantly. So the permeability model was composed of 38 cells 1 meter wide by 1

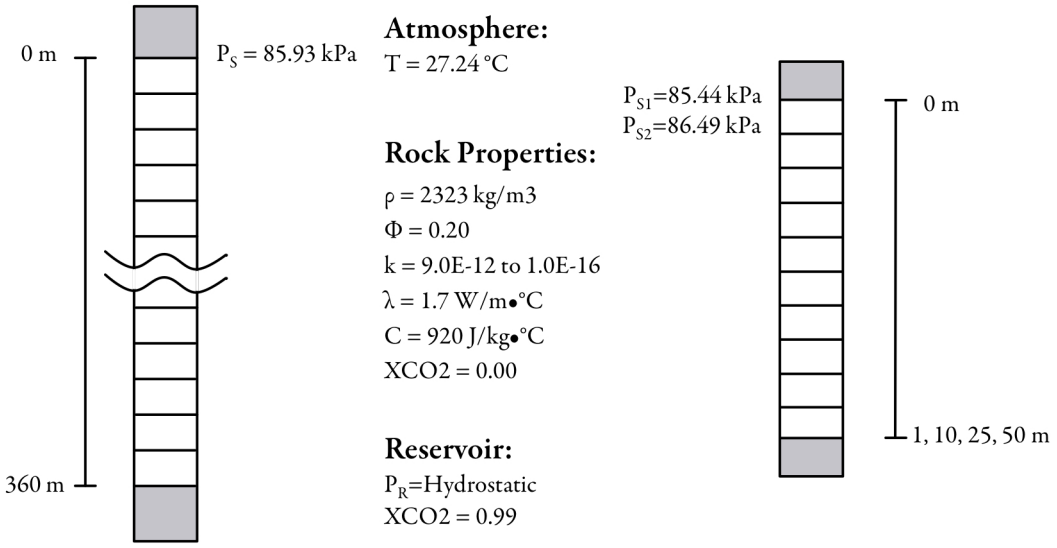

Figure 3.5 Model grid with rock and fluid properties

meter long by 10 meters deep, for a total depth of 380 meters. The 12 cells in the pressure model varied in depth to achieve the total depths of 1, 10, 25, and 50 meters. The top and bottom cells mimic atmospheric conditions and a fully-saturated CO_2 reservoir.

Both models used a Neumann approach, or specific flux boundaries, at the sides of the models. Flux was specified equal to zero to restrict flow to the vertical direction because horizontal flow was beyond the scope of this study.

The pressure differential driven fluid flow in the models was dictated by unequal Dirichlet conditions at the surface and in the reservoir. The permeability model used the average observed barometric pressure, P_S = 85.93 kPa (100.24 kPa adjusted), while the pressure model used the averaged low and high observed barometric pressure, P_{S1} = 85.44 kPa (99.75 kPa adjusted) and P_{S2} = 86.49 kPa (100.8 kPa adjusted). Reservoir pressure for the permeability model was calculated a few different ways. The low reservoir pressure was the minimum pressure needed to induce CO_2 flow to the surface. Hydrostatic pressure was dictated by the elevation of the recharge zone—the elevation of the fault, the elevation of the outcrop of the Navajo sandstone in the San Rafael Swell, and the elevation of the Wingate sandstone in the San Rafael Swell. Two additional reservoir pressures were calculated for graphing purposes to give a more complete picture of reservoir pressure behavior. The model was limited to 360 meters depth because the hydrostatic pressure induced by the highest recharge zone, the Wingate outcrop, created supercritical CO_2 in the Wingate reservoir, but the ECO2N fluid property module cannot resolve a transition of CO_2 from supercritical to subcritical state. So, reservoir pressures were calculated according to their recharge

zone, but depth was limited to 360 meters—the region where CO_2 will have transitioned naturally to a gaseous phase. Reservoir pressure in the pressure model used only two values, the pressures dictated by the elevation of the Navajo and Wingate sandstones in the San Rafael Swell recharge zones.

3.4 Permeability Sensitivity Analysis

A permeability model was generated to assess whether the time necessary for CO_2 to travel from depth to the surface is short enough that a change in reservoir pressure could match the observed lag. The model was run at each reservoir pressure with a range of isotropic permeabilities from 1.0E-16 m^2 to 9.0E-12 m^2, resulting in a surface flux of 1400 g/m^2•day.

3.5 Results of Permeability Sensitivity Analysis

The permeability model exhibited a large range of times, from 3.22E13 seconds (one millions years) to 4.78E9 seconds (151 years), where the target surface flux was reached at steady state (Table 3.1 and Figure 3.6). The results were accompanied by a narrow range of permeabilites, from 8E-16 to 1.5E-15 (Figure 3.7). The minimum reservoir pressure necessary to propagate CO_2 to the surface was 2.36 MPa, which equates to about 65% of hydrostatic pressure. At the minimum reservoir pressure, the pressure differential between the CO_2 reservoir and the atmosphere was 2.27 MPa. However, at the highest reservoir pressure of 7.38 MPa, the pressure differential was 7.29 MPa. Each reservoir pressure is shown to be able to allow sufficient CO_2 to travel to the surface, but the time necessary for the CO_2 to travel from depth to the surface is

Table 3.1 Results of permeability sensitivity analysis at steady state

Hydrostatic from	P_R (MPa)	Permeability (m^2)	Time (s)	Flux (g/m^2•day)
Minimum	2.36	2.00E-15	3.22E+13	1414.04
	2.71	1.50E-15	4.50E+13	1457.70
(Fault)	3.61	8.40E-16	7.04E+13	1415.31
	5.00	5.20E-16	1.06E+13	1392.56
(Navajo)	6.20	3.60E-16	8.19E+12	1414.28
(Wingate)	7.38	8.00E-16	4.78E+09	1441.69

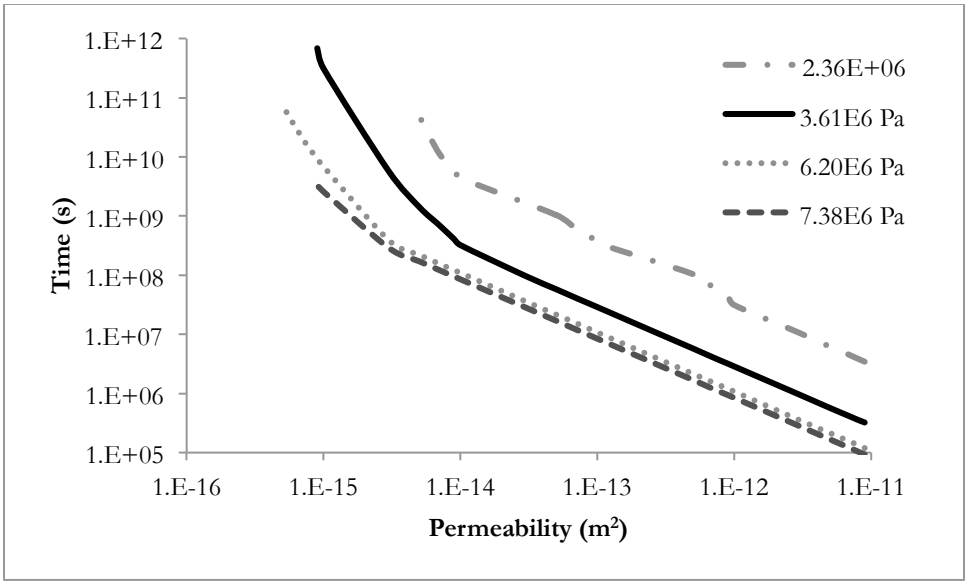

Figure 3.6 Time to reach target flux versus permeability for each reservoir pressure

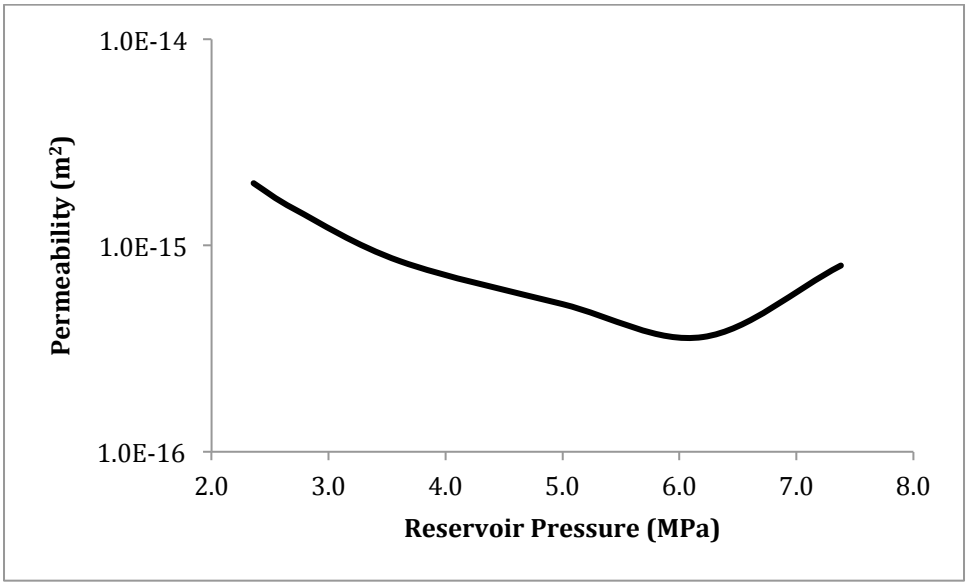

Figure 3.7 Permeability versus reservoir pressure at steady state

much longer than the 21.5-hour response time observed for the directly correlated effect. So, any barometric effect, even an instantaneous transfer of pressure directly to the reservoir, would not be able to change the CO_2 travel time enough to create a 21.5-hour lag in CO_2 flux at the surface. So the barometric effect on flux must happen at a much shallower depth than the depth of the reservoir.

3.6 Pressure Sensitivity Analysis

The direct, time-lagged influence of barometric pressure on the CO_2 fault seepage was addressed by varying barometric pressure in the model. This analysis was used to determine the possibility that an increase in barometric pressure could create an increase in surface CO_2 flux. For simplicity, this system was treated as a perfectly efficient system, where increases in barometric pressure, which cause the earth to compact, propagate through the subsurface to the reservoir, thus increasing reservoir pressure by

an equal amount.

Initial barometric pressure was 85.44 kPa (99.75 kPa adjusted) and initial reservoir pressure (P_{R1}) varied depending on depth of the reservoir (Table 3.2). After pressures were calculated for each cell in the model, the surface pressure was changed to 86.49 kPa (100.8 kPa adjusted) to mimic the observed barometric high. The new reservoir pressure (P_{R2}) was then calculated as the original reservoir pressure (P_{R1}) plus barometric increase of 1050 Pa, mimicking the pressure propagation. The simulation was then run at each depth to find permeabilities that allowed CO_2 to reach the surface in roughly 21.5 hours.

3.7 Results of Pressure Sensitivity Analysis

The pressure sensitivity analysis results revealed that an increase in barometric pressure can exhibit an increase in surface flux. A narrow range of permeabilities, from 1.0E-13 to 1.8E-12, resulted in the target surface flux being reached in roughly 7.74E4 seconds (21.5 hours) at every depth (Table 3.3). The resulting permeability range encountered in these simulations is higher than that of the surrounding rock, but it has been suggested that the fault aslo has a higher permeability than the formations it traverses (Evans et al., 2004; Shipton et al., 2004). The effect of depth versus

Table 3.2 Pressure model reservoir pressures

Depth (m)	Navajo P_{R1} (Pa)	Navajo P_{R2} (Pa)	Wingate P_{R1} (Pa)	Wingate P_{R2} (Pa)
1	101495	102545	106500	107550
10	246349	247399	277400	278450
25	487773	488823	565300	566350
50	890146	891196	1045000	1046050

Table 3.3 Results of pressure sensitivity analysis

Hydrostatic at	Depth (m)	Permeability (m^2)	Time (s)	Time (hrs)	Flux (g/m^2•day)
Navajo	1	1.50E-13	7.42E+04	20.61	3856.08
	10	4.50E-13	7.61E+04	21.14	3856.08
	25	1.00E-12	8.14E+04	22.61	3856.08
	50	2.00E-12	7.88E+04	21.89	3856.08
Wingate	1	1.00E-13	8.62E+04	23.94	3856.08
	10	3.50E-13	7.70E+04	21.39	3856.08
	25	8.00E-13	7.90E+04	21.94	3856.08
	50	1.50E-12	8.08E+04	22.44	3856.08

permeability seems to be greatest up to about 25 meters, since the graph of log permeability versus depth begins to flatten out in that range for both artesian pressures (Figure 3.8). Both the Wingate driven CO_2 and the Navajo driven CO_2 seem to follow a similar trend, but the Navajo pressures follow a higher permeability range. This result coincides with the observed data and suggests that the barometric effect decreases with depth and that the observed cyclic variations in CO_2 leakage is due to pressure changes in the subsurface at relatively shallow depths of less than 25 meters.

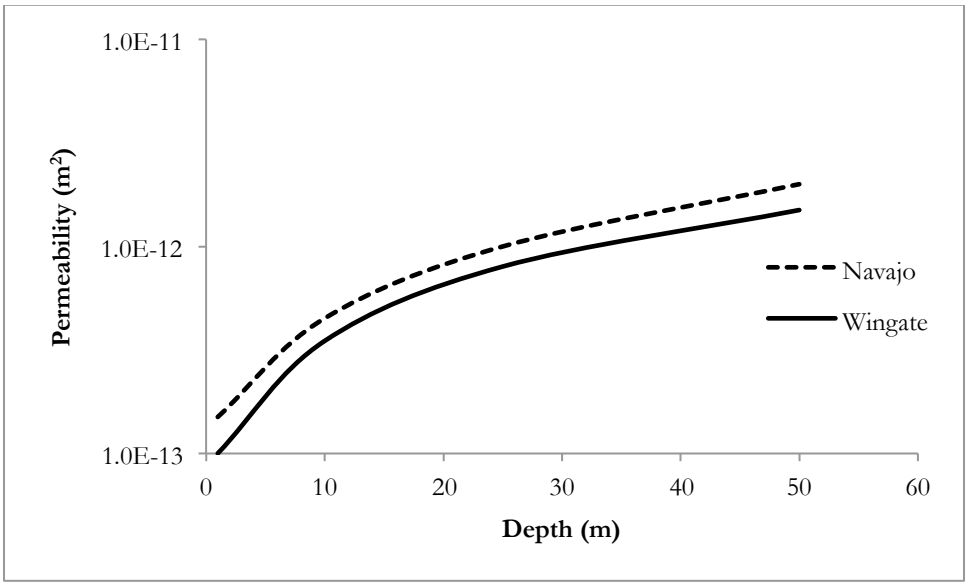

Figure 3.8 Log permeability versus depth

CHAPTER 4

SUMMARY AND CONCLUSIONS

The gas flux measured along the Little Grand Wash fault is influenced by barometric pressure via two mechanisms. The first mechanism involves an immediate and inverse correlation that was observed over short time intervals. As atmospheric pressure increases, CO_2 flux decreases and vice versa. The second mechanism, involving the interaction between atmospheric pressure and the earth, exhibits a direct correlation, but with a time delay before the effect is manifested through CO_2 surface flux. As barometric pressure increases, CO_2 flux also increases with a 21.5-hour lag.

Results from the permeability model demonstrated the possibility that a CO_2-charged aquifer could produce a flux response at a surface elevation comparable to the leakage site at the Crystal Geyser. However, fluctuations in barometric pressure likely do not produce a pressure gradient that propagates quickly enough to the depth of the Wingate formation sufficient to motivate CO_2 to a 21.5-hour response time as observed.

The pressure model verified the possibility that an increase in barometric pressure can produce an increase in surface flux lagged by 21.5 hours, similar to the observed data at the Crystal Geyser site. The barometric effect was shown to decrease with depth and is most pronounced at depths of less than 25 meters.

Two one-dimensional computer models were created to deal with the two separate

mechanisms involved in the variations in CO_2 flux that were identified from the field-obtained data. The first columnar model, or permeability model, which addresses the time needed for CO_2 to travel from reservoir depth to the surface, varied the isotropic rock permeability in order to obtain a range of values that would still be able to emit a CO_2 surface flux of roughly 1400 g/m^2•day.

The second one-dimensional columnar model, or pressure model, used to express the direct, yet time-delayed phenomenon, varied the barometric pressure. Changes in barometric pressure propagate through the subsurface and charge the reservoir with an equal change in pressure. These simulations were used to assess a range of depths and associated permeabilities that allowed the model to emit a CO_2 surface flux of roughly 1400 g/m^2•day with a 21.5-hour lag, which matched the observed data.

Knowing that short-term CO_2 surface flux is affected by barometric pressure, but only in the shallow subsurface, suggests that deep-saline CO_2 storage is likely to be safe from the short-term effects of other body forces that affect the earth, like earth tides.

Further studies on the effect of earth tides on leakage rates of surface CO_2 flux would help to solidify understanding of the dynamics of fault systems and their effect on surface CO_2 leakage. Additional studies using longer-term data and/or a two or three-dimensional system would be beneficial in further understanding these phenomena, as well. Other influences such as soil moisture and air temperature could also reveal information on the intricacies of this system.

REFERENCES

Baer, J. L.; Rigby, J. K. Geology of the Crystal Geyser and Environmental Implications of its Effluent, Grand County, Utah. *Utah Geol*., **1978,** *5*, 125–130.

Batu, V. *Aquifer Hydraulics: A Comprehensive Guide to Hydrogeologic Data Analysis*; Wiley: New York, 1998.

Burnside, N. M.; Shipton, Z. K.; Dockrill, B.; Ellam, R. M. Man-Made Versus Natural CO_2 Leakage: A 400 K.Y. History of an Analogue for Engineered Geological Storage of CO_2. *Geology*, **2013,** *41*, 471–474.

Campbell, J. A. *Carbon Dioxide Resources of Utah*; Report of Investigations No. 125 for Utah Geological and Mineral Survey: Salt Lake City, Utah, June 1978.

Campbell, J. A.; Baer, J. L. Little Grand Wash Fault-Crystal Geyser. In *Oil and Gas Fields of the Four Corners Area*; Four Corners Geological Society: Durango, CO, 1978; Vols. 1–2, pp. 666–669.

Dockrill, B.; Shipton, Z. K. Structural Controls on Leakage from a Natural CO_2 Geologic Storage Site: Central Utah, U.S.A. *J. Struct. Geol.*, **2010,** *32*, 1768–1782.

DOE *Report of the Interagency Task Force on Carbon Capture and Storage* [Online]; U.S. Department of Energy, 2010. http://energy.gov/sites/prod/files/2013/04/f0/CCSTaskForceReport2010_0.pdf (accessed Oct 7, 2012).

Evans, J. P.; Heath, J.; Shipton, Z. K.; Kolesar, P. T.; Dockrill, B.; Williams, A.; Kirchner, D.; Lacmar, T. E.; Nelson, S. T. Natural Leaking CO_2-Charged Systems as Analogs for Geologic Sequestration Sites. Proceedings of the Third Annual Conference on Carbon Capture and Sequestration, Alexandria, VA, May 3–6, 2004.

Freeze, R. A. Henry Darcy and the Fountains of Dijon. *Groundwater*, **1994,** *32*, 23–30.

Gale, J. Geological Storage of CO_2: What Do We Know, Where Are the Gaps and What More Needs to Be Done? *Energy*, **2004,** *29*, 1329–1338.

Glennon, J. A.; Pfaff, R. M. The Operation and Geography of Carbon Dioxide-Driven, Cold-Water "Geysers." *The GOSA Transactions*, **2005,** *9*, 184–192.

Gouveia, F.; Friedmann, S. J. (2006). *Timing and Prediction of CO_2 Eruptions from Crystal Geyser, UT*; Technical Report for Lawrence Livermore National Laboratory. Livermore, CA, May 2006.

Gunter, W.D.; Wong, S.; Cheel, D.B.; Sjostrom, G. Large CO_2 Sinks: Their Role in the Mitigation of Greenhouse Gases from an International, National (Canadian) and Provincial (Alberta) Perspective. *Appl. Energy*, **1998,** *61*, 209–227.

Gupta, N.; Sass, B.; Sminchak, J.; Naymik, T.; Berman, T. Hydrodynamics of CO_2 disposal in a deep saline formation in the midwestern United States: In *Greenhouse Gas Control Technologies*; Eliasson, B., Riemer, P.W.F., Wokaun, A., Eds.; Elsevier: Oxford, 1999; pp 157–162.

Hare, P. W.; Morse, R. E. Water-Level Fluctuations Due to Barometric Pressure Changes in an Isolated Portion of an Unconfined Aquifer. *Groundwater*, **1997,** *35*, 667–671.

Heath, J. E. Hydrogeochemical Characterization of the Leaking Carbon Dioxide-Charged Fault Zones in East-Central Utah. M.S. Thesis, Utah State University, 2004.

Hintze, L. F. *Geologic Maps of Beaver, Millard, Washington, Utah, and Lincoln Counties*; Geologic History of Utah, Alma J. Hintze Memorial, Special Publication 7; Brigham Young University Geological Studies: Provo, UT, 1993.

Hood, J. W.; Patterson, D. J. Bedrock Aquifers in the Northern San Rafael Swell Area, Utah, with Special Emphasis on the Navajo Sandstone. Technical Publication No. 78; USGS, 1984; Plate 5.

IPCC. *IPCC Special Report on Carbon Dioxide Capture and Storage*, Prepared by Working Group III of the Intergovernmental Panel on Climate Change, Metz, B., Davidson, O., de Coninck, H. C., Loos, M., Meyer, L. A., Eds.; Cambridge: Cambridge, 2005.

IPCC. *Climate Change 2007: The Physical Science Basis. Contribution of Working Group I to the Fourth Assessment Report of the Intergovernmental Panel on Climate Change*; Solomon, S., Qin, D., Manning, M., Chen, Z., Marquis, M., Averyt, K. B., Tignor M., Miller, H. L., Eds.; Cambridge: Cambridge, 2007.

Jeandel, E.; Battani, A.; Sarda, P. Lessons Learned from Natural and Industrial Analogues for Storage of Carbon Dioxide. *Int. J. Greenhouse Gas Control*, **2010,** *4*, 890–909.

Kampman, N.; Bickle, M. J.; Maskell, A.; Chapman, H. J.; Evans, J. P.; Purser, G.; Zhou, Z.; Schaller, M. F.; Gattacceca, J. C.; Bertier, P.; Chen, F.; Turchyn, A. V.; Assayag, N.; Rochelle, C.; Ballentine, C. J.; Busch, A. Drilling and Sampling a Natural CO_2 Reservoir: Implications for Fluid Flow and CO_2-Fluid–Rock Reactions During CO_2 Migration Through the Overburden. *Chem. Geol.*, **2014,** *369*, 51–82.

Kelsey, M. R. *Hiking and Exploring Utah's San Rafael Swell*, 4th ed.; Kelsey Publishing: Provo, UT, 2014.

Mills, M. P. *Unleashing the North American Energy Colossus: Hydrocarbons Can Fuel Growth and Prosperity*; Manhattan Institute for Policy Research: New York, 2012.

Nicol, A.; Carne, R.; Gerstenberger, M.; Christophersen, A. Induced Seismicity and its Implications for CO_2 Storage Risk. *Energy Procedia*, **2011,** *4*, 3699–3706.

Oldenburg, C. M.; Unger, A. J. On Leakage and Seepage from Geologic Carbon Sequestration Sites: Unsaturated Zone Attenuation. *Vadose Zone J.*, **2003,** *2*, 287–296.

Pearce, J.; Holloway, S.; Wacker, H.; Nelis, M.; Rochelle, C.; Bateman, K. Natural Occurrences as Analogues for the Geological Disposal of Carbon Dioxide. *Energy Convers. Manage.*, **1996,** *37*, 1123–1128.

Pruess, K.; Oldenburg, C.; Moridis, G. *TOUGH2*, version 2.0; Lawrence Berkeley National Laboratory: Berkeley, CA; 1999.

Pruess, K. *ECO2N: A TOUGH2 Fluid Property Module for Mixtures of Water, NaCl, and CO_2*; Lawrence Berkeley National Laboratory: Berkeley, CA; 2005.

Rasmussen, T. C.; Crawford, L. A. Identifying and Removing Barometric Pressure Effects in Confined and Unconfined Aquifers. *Groundwater*, **1997,** *35*, 502–511.

Shipton, Z. K.; Evans, J. P.; Kirchner, D.; Kolesar, P. T.; Williams, A. P.; Heath, J. Analysis of CO_2 leakage through "low-permeability" faults from natural reservoirs in the Colorado Plateau, southern Utah. In: Baines, S. J.; Worden, R. H. Eds.; *Geological Storage of Carbon Dioxide.* Geological Society; London, 2004; Special Publications 233, pp 43–58.

Spane, F. *Effects of Barometric Fluctuations on Well Water-Level Measurements and Aquifer Test Data*. Technical Report for Pacific Northwest National Laboratory: Richland, WA, December 1999.

Vrolijk, P.; Myers, R.; Sweet, M. L.; Shipton, Z. K.; Dockrill, B.; Evans, J. P.; Heath, J.; Williams, A. P. Anatomy of reservoir-scale normal faults in central Utah: Stratigraphic controls and implications for fault zone evolution and fluid flow. In *Interior Western United States*; Pederson, J. L; Dehler, C. M. Eds.; GSA Field Guides: Boulder, CO, 2005; Vol. 6, pp 261–282.

Waltham, T. Crystal Geyser - Utah's Cold One. *Geology Today*, **2001,** *17*, 22–24.

Weir, G.; White, S.; Kissling, W. Reservoir Storage and Containment of Greenhouse Gases. *Energy Convers. Manage.*, **1995,** 36, 531–534.

White, S. P.; Weir, G. J.; Kissling, W. M. Numerical Simulation of CO_2 Sequestration in Natural CO_2 Reservoirs on the Colorado Plateau. Proceedings of the First National Conference on Carbon Sequestration, Washington, DC, May 14–17, 2001.

Wilkinson, M.; Gilfillan, S. M. V.; Haszeldine, R. S.; Ballentine, C. J. Plumbing the Depths: Testing Natural Tracers of Subsurface CO_2 Origin and Migration, Utah, USA. In *Carbon Dioxide Sequestration in Geological Media — State of the Science*; Grobe, M.; Pashin, J. C.; Dodge, R. L., Eds.; AAPG Studies in Geology: Tulsa, 2009; Vol. 59, pp 619–634.